# SIMULATION OF THE THERMOELECTRICALLY GENERATED MAGNETIC FIELD IN A SC NINE-CELL CAVITY

J. Köszegi†, O. Kugeler, J. Knobloch, Helmholtz-Zentrum Berlin, Germany

*Abstract*

Several studies showed that thermocurrents generate a magnetic field in a horizontal cavity test assembly or cryomodul, which may get trapped during the superconducting (sc) phase transition [1-3]. The trapped flux causes additional dissipation in the order of 1 to10 nΩ during operation and can therefore significantly degrade the quality factor in a TESLA cavity.

We simulated the distribution of the generated magnetic field over the whole cavity-tank system for an asymmetric temperature distribution. The asymmetry allows the field to penetrate the RF surface which would be field free in the symmetric case. The calculated results complemented a direct measurement of trapped magnetic flux inside the cavity with a small number of field probes.

Finally, the obtained data was combined with RF measurements in three passband modes to determine the overall distribution of trapped magnetic flux due to thermocurrents.

## NUMERICAL SIMULATION

### *Setup*

Figure 1 presents the model which was used to simulate the magnetic field in the cavity-tank-system. It includes the niobium cavity, the LHe tank (titanium) and the magnetic shield. A ring was added to the helium vessel head to account for the resistance of the (not included) bellow [4]. The total resistance was tuned using this ring based on the experimental data from the vertical test in Reference [5]. The temperature dependent material properties heat capacity, thermal conductivity, electrical conductivity and thermopower were taken from References [6-8].

Based on the cool down scheme in horizontal operation, where the liquid helium is filled via a filling line in the bottom left of the tank, two temperature gradients were introduced in the simulations: First a gradient from left to right which drove the thermocurrent. Second, a gradient from bottom to top which must be included because it breaks the symmetry of the current distribution. Without the second gradient, no magnetic field would be present at the RF surface inside the cavity [2, 3].

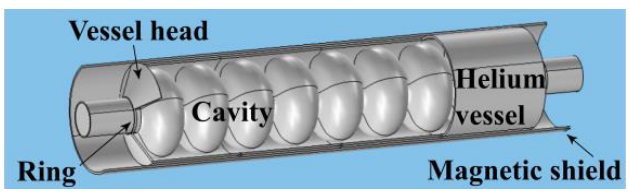


Figure 1: Model of cavity, tank with ring for adjustment of electrical resistance and magnetic shield.

† julia.koeszegi@helmholtz-berlin.de

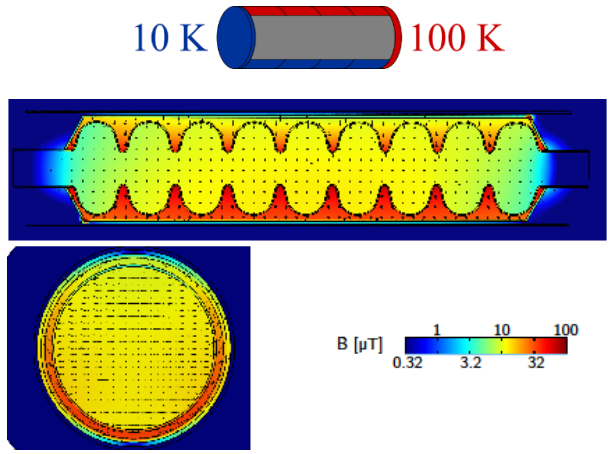


Figure 2: Magnetic field inside cavity and tank in a logarithmic scale asymmetric temperature boundaries (displayed on top). The black arrows indicate the magnetic field vectors that point into and out of the paper in the top figure and from left to right in the bottom figure.

### *Results*

Figure 2 shows the magnetic field obtained for asymmetric temperature boundaries over the whole length of the cavity. The vessel heads were set to 10 K and 100 K for the first gradient and, in addition, the bottom quarter of the helium tank was set to 10 K and the top quarter to 100K for the second gradient.

The resulting distribution is comparable to previously presented simulations [2, 3]. In addition, we found that the magnetic field inside the cavity is more homogeneous due to the magnetic shield which is placed closely around the helium vessel.

Furthermore, the field inside the cavity is orientated orthogonal to the bottom to top gradient. Since the vessel heads are set to a constant temperature, the asymmetry and hence magnetic field in cells 1 and 9 are reduced. In the cells 2 to 8, it ranges from 8 μT to 14 μT. The maximum in each cell is at the bottom and the field decreases towards the top. This result has the correct magnitude to explain the increased residual resistance in the RF tests [1-3].

## DIRECT MEASUREMENT

### *Setup*

The magnetic field which was calculated between the tank and the cavity agreed with the experimental data. The field inside the cavity at the RF surface however was determined by the asymmetry. Hence the simulation has to be verified by a measurement.



ISBN 978-3-95450-182-3

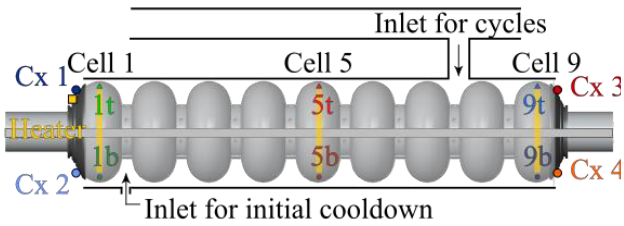


Figure 3: Positions of four Cernox sensors outside and six fluxgate magnetometers inside the cavity.

For that purpose, a similar TESLA cavity was equipped with six fluxgate magnetometers from the inside. The cavity was provided by DESY. The setup of the sensors is shown in Figure 3. The sensors were placed in the bottom and in the top of the equator in cells 1, 5 and 9.

### *Results*

The presented setup was used to track the change in magnetic field during warm up and cool down of nine thermal cycles. Figure 4 displays the data of one Cycle 4 as an example. The six FGs were read out by four read out units hence only four probes could be read simultaneously. In addition, Figure 5 shows the magnetic field data during the cool down period of Cycle 8.

At the beginning of each cycle, the LHe was evaporated. The temperatures increased slightly but no change in magnetic field occurred. Once the tank was empty, the probes show a small increase in magnetic field due to thermoelectric current during the heating period. The signal was most distinct in cell 1 where the FGs reached about 2 µT. The field values were, however, low compared to the values, which were measured in the space between cavity and tank in the previous test [9] and smaller than simulated. The numbers indicate that the heating created an almost symmetric temperature distribution, which resulted in a high thermoelectrically generated magnetic field in the tank but almost no field inside the cavity. The situation changed drastically once the cooldown started. A strong asymmetry was introduced by the cold gas and the magnetic field inside the cavity rapidly increased. FG1b in cell 1 reached a maximum in absolute field of 6 µT. The thermoelectric field was less pronounced in the other cells though it also amounted to 1 to 2 µT. The signal was strongest in cell 1 because it was closest to the heater which was positioned off-center and hence contributed to the bottom-top asymmetry. Since the FGs inside the cavity registered only asymmetric induced magnetic field, the measured field before the phase transition was maximum in cell 1 and smaller in cells 5 and 9.

The sc phase transition started in cell 9. The transition significantly changed the magnetic signal because the establishing sc area had no dc resistance and therefore introduced the strongest bottom-top asymmetry for the thermocurrent. Hence, the measured field inside the cavity also rapidly increased and was (partially) trapped. The amount of trapped magnetic flux in the sc state was evaluated for all six sensors after the transition was completed and the data was plotted versus the temperature differences at the onset of sc phase transition.

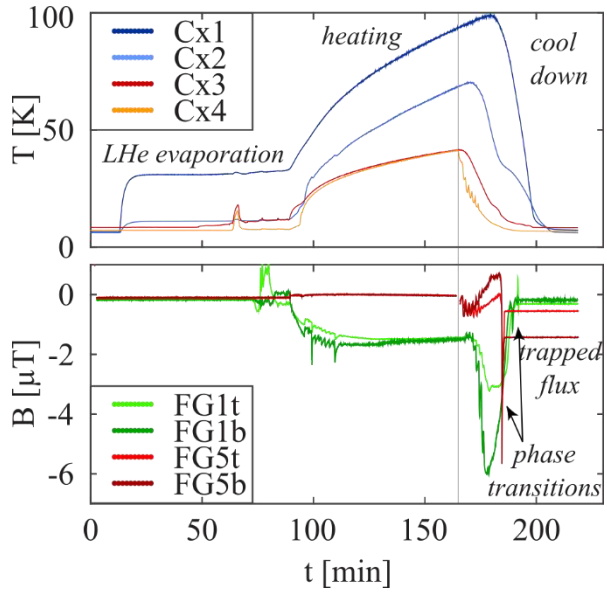


Figure 4: Signal of Cernox sensors and fluxgates during thermal cycle 4. The vertical black line indicates when the LHe refilling was started.

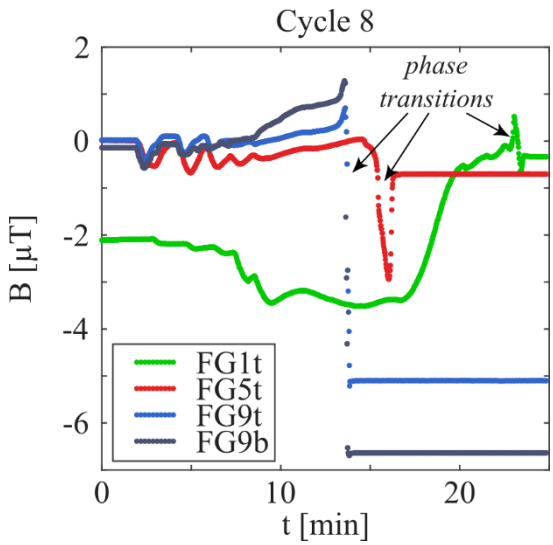


Figure 5: Magnetic signal during cool down of Cycle 8.

The result is presented in Figure 6. It shows that the simulation of compete asymmetry given in Figure 2 provides a reasonable approximation for the highest values of trapped flux which were obtained in cell 9 – the cell which transition first (8.3 µT for $\Delta T$ = 71 K). The other cells showed lower values of trapped flux. The decrease can be explained by the time lag of the transition from cell to cell. By the time when cells 5 and 1 transitioned, the temperature difference between the cavity-tank-joints had already reduced. The time lag between transitions in cells 1 and 9 was approximately 5 to 10 min for the various thermal cycles which was enough time for the temperature difference to drop several 10 K. Finally, cell 1 which transitioned last exhibited only a maximum of 0.35 µT of trapped flux and therefore showed no drastic increase due to thermocurrents for any thermal cycle.




ISBN 978-3-95450-182-3

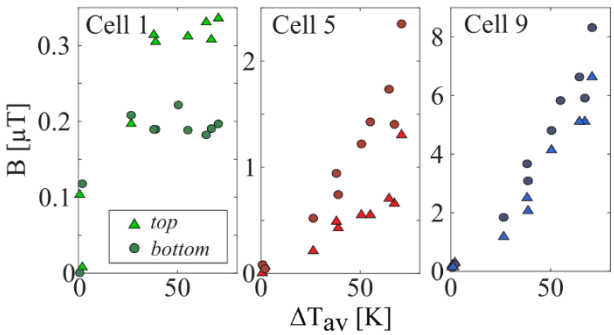


Figure 6: Direct measurement of the trapped flux inside the cavity by six fluxgates.

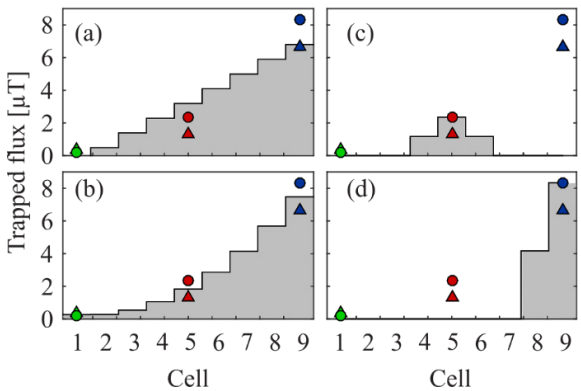


Figure 7: Directly measured trapped flux in cells 1, 5 and 9 together with conceivable distributions of trapped magnetic flux in all nine cells for one example cycle.

In addition, we found that the niobium in the bottom trapped more flux compared to the top in cells 5 and 9. This might also be caused by a time lag because all cells transitioned bottom first. However, it must be considered that the distribution of the thermocurrent field was changed by the established sc area as shown by simulation in Ref. [6].

Based on the direct measurement of the trapped magnetic flux in three cells and on the simulations we constructed conceivable distributions of trapped flux for all nine cells. Figure 7 shows a linear (a) and a quadratic (b) distribution along the cells. Furthermore, we added models of trapped flux including only the middle (c) or end (d) cells for comparison.

### *Comparison to RF Results*

Ref. [2] presented measurements of the surface resistance in three passband modes. It included an analysis of the $R_{res}$ in the 8/9 π and 1/9 π modes as a function of the π mode $R_{res}$. The data allowed us to access the distribution of the surface resistance over the whole cavity. The results are reprinted in Figure 8. We added the four interpolations of Figure 7 to show how they match with the RF results. The Figure shows that distributions which consider only selected cells (c, d) do not fit with the RF data at all. The continuous interpolations (a, b), however, give reasonable results where the linear distribution fits better for the 1/9 π mode while the quadratic distribution fits better for the 8/9 π mode which hints that the actual distribution is somewhere in between the two.

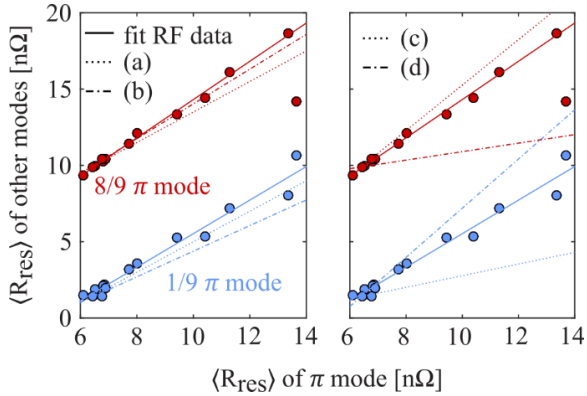


Figure 8: RF data from Ref. [2] compared to conceivable distributions of trapped flux.

## CONCLUSION

We simulated the magnetic field produced by thermocurrents in a fully equipped TESLA nine-cell cavity including the magnetic shield. Direct measurement of the trapped flux showed that the simulation was a good approximation of the trapped flux for the first cell which transitioned into the sc state. The cells which transitioned later showed lower levels of trapped flux because the temperature difference driving the thermocurrent decreased during the time that the sc phase needed to expand over the length of the cavity (several minutes). A combination of the results with previous RF tests showed that trapped flux by thermocurrents must be considered as a global effect which degrades the whole cavity and is not limited to certain cells or areas though it decreases over the cavity's length.

## REFERENCES

[1] J. Vogt, O. Kugeler, and J. Knobloch, "Impact of cool-down conditions at Tc on the superconducting RF cavity quality factor," *Phys. Rev. ST Accel. Beams*, vol. 16, p. 102002, Oct 2013.

[2] J. Vogt, O. Kugeler, and J. Knobloch, "High-Q operation of superconducting RF cavities: Potential impact of thermocurrents on the RF surface resistance," *Phys. Rev. ST Accel.* Beams, vol. 18, p. 042001, Apr 2015.

[3] R. Eichhorn *et al.,* "Thermocurrents and their role in high Q cavity performance," *Phys. Rev. Accel. Beams*, vol. 19, p. 012001, Jan 2016.

[4] A. Crawford, " A study of thermocurrent induced magnetic fields in ILC cavities", arXiv:1403.7996v1, 2013.

[5] J. Vogt *et al.,* "Fermilab studies of quality factor changes of a N doped cavity from vertical to dressed horizontal test", TTC meeting, KEK, 2014.

[6] J. Köszegi, PhD thesis. Universität Siegen, 2017.

[7] J. Jensen, R. Stewart, W. Tuttle, H. Brechna and A. Prodell, "Selected cryogenic data notebook, vol. 2," Brookhaven National Laboratory, 1980.

[8] M. Merio and T. Peterson, "Material properties for engineering analysis of SRF cavities," Fermilab Specification: 5500.000-ES-371110, 2011.

[9] O. Kugeler *et al.,* "Horizontal testing and thermal cycling of an N-doped TESLA-type cavity", SRF'15, Whistler, Canada, September 2015, MOPB019, p.125.